NSD2 silencing alleviates pulmonary arterial hypertension by inhibiting trehalose metabolism and autophagy

Xue-liang Zhou[1, *], Zhi-bo Liu[1, *], Rong-rong Zhu[2, *], Huang Huang[1], Qi-rong Xu[1], Hua Xu[1], Liang Zeng[1], Yun-yun Li[1], Cha-hua Huang[3], Qi-cai Wu[1], Ji-chun Liu[1, #]

1 Department of Cardiac Surgery, The First Affiliated Hospital, Nanchang University, Nanchang, Jiangxi 330006, China

2 Department of Obstetrics and Gynecology, Affiliated Hospital of traditional Chinese and Western medicine, Jiangxi University of traditional Chinese Medicine, Nanchang 330006, China

3 Department of Cardiovasology, Second Affiliated Hospital, Nanchang University, Nanchang, Jiangxi 330006, China

* These authors contributed equally to this work

#Correspondence: Ji-chun Liu, Department of Cardiothoracic Surgery, The First Affiliated Hospital, Nanchang University, Nanchang, Jiangxi, 330006, China ; E-mail: liujichun999@163.com

Running title: **NSD2 mediates metabolic reprogramming in PAH**

Clinical perspective

- Pulmonary arterial hypertension (PAH) has been proposed to share similarity to oncogenesis. NSD2-mediated metabolic reprogramming regulates oncogenesis but its role in PAH has never been investigated
- Here we show that silencing of NSD2 effectively ameliorated MCT-induced PAH and right ventricle dysfunction, and partially reversed pathological remodeling of pulmonary artery and right ventricular hypertrophy. In addition, silencing of NSD2 markedly reduced the di-methylation level of H3K36 in pulmonary artery. Metabolomics analysis indicated that trehalose showed the most significant change in lung tissue. NSD2-regulated trehalose mainly affected ABC transporters, mineral absorption, protein digestion and absorption, metabolic pathways and aminoacyl-tRNA biosynthesis. Furthermore, silencing of NSD2 inhibited autophagy in pulmonary artery, consistent with the change in trehalose metabolism.
- We reveal a new role of NSD2 in the pathogenesis of PAH related to the regulation of trehalose metabolism via increasing histone di-methylation. NSD2 is a promising target for PAH therapy.

Abstract

Nuclear receptor binding SET domain 2 (NSD2)-mediated metabolic reprogramming has been demonstrated to regulate oncogenesis via catalyzing the methylation of histones. This study aimed to investigate the role of NSD2 mediated metabolic abnormality in pulmonary arterial hypertension (PAH). Monocrotaline (MCT)-induced PAH rat model was established and infected with adeno-associated virus carrying shRNA targeting NSD2. Hemodynamic parameters, ventricular function and pathology were evaluated by microcatheter, echocardiography and histological analysis. Metabolomics changes in lung tissue were analyzed by liquid chromatography-mass spectrometry (LC-MS). The results showed that silencing of NSD2 effectively ameliorated MCT-induced PAH and right ventricle dysfunction, and partially reversed pathological remodeling of pulmonary artery and right ventricular hypertrophy. In addition, silencing of NSD2 markedly reduced the di-methylation level of H3K36 and inhibited autophagy in pulmonary artery. Non-targeted LC-MS based metabolomics analysis indicated that trehalose showed the most significant change in lung tissue. NSD2-regulated trehalose mainly affected ABC transporters, mineral absorption, protein digestion and absorption, metabolic pathways and aminoacyl-tRNA biosynthesis. In conclusion, we reveal a new role of NSD2 in the pathogenesis of PAH related to the regulation of trehalose metabolism and autophagy via increasing the di-methylation level of H3K36 (H3K36me2). NSD2 is a promising target for PAH therapy.

Keywords: Pulmonary arterial hypertension; NSD2; H3K36; Methylation; Metabolism; Trehalose; Autophagy

1 Introduction

Pulmonary arterial hypertension (PAH) is a complex and progressive cardiopulmonary disorder characterized by increased pulmonary vascular resistance (PVR) and pulmonary artery pressure (PAP), ultimately leading to the dysfunction and failure of the right ventricle and death. Histological aspects of PAH include intimal hyperplasia, medial hypertrophy, adventitial proliferation, and pathognomonic plexiform lesions. Notably, PAH demonstrates several analogous features with carcinogenesis, including apoptotic resistance, pathological hyperproliferation and excessive migration of pulmonary smooth muscle cell (SMC), endothelial cell (EC) and fibroblast, metabolic reprogramming, inflammation and fibrosis [1]. In addition, PAH shares similar metabolic abnormalities with oncogenesis that account for the hyperproliferative, apoptosis resistant, and pro-survival phenotype of pulmonary vasculature, angiogenesis, cell migration and vessel stiffening and fibrosis [2]. For example, aberrant metabolism has been proposed to reduce right ventricle contractility and promote adventitial fibroblast, infiltrating macrophage and perivascular mononuclear cells pro-inflammatory, hyperproliferative and pro-fibrotic phenotype[3]. In cancer and PAH, the mechanisms involved in mitochondrial metabolic abnormalities and glycolysis include but are not limited to fragmented mitochondria, decreased nitric oxide (NO) synthesis, reduced expression of electron transport chain complexes I, III, and IX, epigenetic silencing of mitochondrial superoxide dismutase 2 (SOD2), altered reactive oxygen species (ROS) production, pyruvate dehydrogenase kinase (PDK) induced pyruvate dehydrogenase (PDH) inhibition, and the expression of pro-survival and proangiogenic hypoxia-inducible factor (HIF)-1[3-5].

Nuclear receptor binding SET domain 2 (NSD2)/multiple myeloma SET domain (MMSET)

is a member of histone methyltransferase (HMTase) family, and acts as an epigenetic modifier through methylating lysine residues on histone to change chromatin accessibility[6,7]. Recent studies showed that NSD2 was translocated, amplified, deleted or somatically mutated in multiple types of cancer, suggesting a role in oncogenesis[8-10]. High NSD2 expression was associated with tumor aggressiveness, drug resistance, recurrence and poor prognosis [8,11,12]. NSD2 can catalyze the mono-methylation of H3K36 (H3K36me1), di-methylation of H3K36 (H3K36me2) and H3K20 (H3K20me2), and tri-methylation of H3K36 (H3K36me3), H3K4 (H3K4me3) and H3K20 (H3K20me3) [13]. The overexpression of NSD2 in breast and prostate cancer led to aberrant high level of di- and/or tri-methylation of H3K36, indicating that H3K36me2 and H3K36me3 are the main functional products of NSD2[12,14].

NSD2 participates in metabolic reprogramming (aerobic glycolysis) in tamoxifen-resistant breast cancer [12]. Mechanistically, NSD2 was recruited to di-methylated H3K36 (H3K36me2) at the promoters of hexokinase 2 (HK2) and glucose-6-phosphate dehydrogenase (G6PD), two key enzymes of glycolysis and the pentose phosphate pathway (PPP). Overexpression of NSD2 conferred breast cancer cells hormone-independent proliferative activities[12], and promoted osteosarcoma cell proliferation and invasion[15]. However, it remains unknown whether NSD2 participates in metabolic reprogramming of pulmonary vasculature in PAH.

We hypothesized that NSD2 drives the pathogenesis of PAH by linking histone methylation to metabolic reprogramming, leading to hyperproliferative, apoptosis resistant and survival capability of the cells in pulmonary vasculature. In this study, we established monocrotaline (MCT)-induced rat model of PAH and adopted adeno-associated virus (AAV) mediated short hairpin RNA (shRNA) silencing of NSD2 to determine the role of NSD2 in PAH.

2 Materials and Methods

2.1 Animals and reagents

Male Sprague-Dawley (SD) rats (300-350 g body weight) were obtained from Slaccas Co. Ltd. (Shanghai, China). All animal studies were performed at Experimental Animal Center of Nanchang University in accordance with the Guideline of US National Institutes of Health (NIH) and approved by the Institutional Committee for Use and Care of Laboratory Animals of Nanchang University. Monocrotaline was purchased from Selleck (Cat. S3812, Shanghai, China). To establish PAH rat model, SD rats were given intraperitoneal injection of saline (sham, n=6) or MCT at 60 mg/kg body weight (BW) (n=6). The BW changes were monitored from 21 to 35 days for all experimental groups.

BCA protein assay kit was obtained from Pierce (Rockford, IL, USA). Rabbit anti-NSD2 antibody (ab223694) and mouse anti-α-smooth muscle actin (α-SMA, ab5694) antibody were purchased from Abcam (Cambridge, UK). Rabbit anti-H3K4me1/2/3, anti-H3K36me1/2/3 and anti-Histone H3 antibodies were obtained from Santa Cruz Biotechnology (Dallas, TX, USA). Rabbit anti-LC3I/II, anti-p62, anti-phos-AMPK and anti-AMPK, and mouse anti-Beclin1were purchased from Cell Signaling Technology (Cambridge, MA, USA). Goat anti-rabbit IgG, goat anti-mouse IgG and rabbit anti-HRP-GAPDH were obtained from KangChen Bio (Shanghai, China). Enhanced chemiluminescent (ECL) reagent was from Amersham (Piscataway, NJ, USA).

2.2 Generation of recombinant AAV-shNSD2

Adeno-associated virus-2 vector (AAV2, Stratagene, La Jolla, CA, USA) carrying NSD2

shRNA 5’ CACGAATGTTCTGTATTCCTCAGCA-3’ (named AAV-shNSD2) and carrying scramble sequence (named AAV-null) were constructed by Genelily Biotech (Shanghai, China). AAV-shNSD2 and AAV-null were then packaged with pHelper and pAAV-RC in modified AAV 293 cells to produce recombinant virus particles. The titer was determined by real-time PCR. 5×10^{12} of AAV-shNSD2 were used to infect the rats by tail vein.

2.3 Echocardiographic measurements

Echocardiographic measurements of pulmonary artery acceleration time normalized to cardiac cycle length (PAAT/CL), Right ventricular end diastolic dimension (RVEDD), RV end-diastolic systolic dimension (RVESD), Right ventricular end diastolic volume (RVEDV), RV end-diastolic systolic volume (RVESV), RV cardiac output (RVCO), right ventricular wall thickness (RVWT), interventricular septum thickness (IVS), right ventricular ejection fraction (RVEF) and right ventricular fractional shortening (RVFS) were performed for all experimental groups. Anesthesia was induced with 3% isoflurane gas and maintained with 1.0% to 1.5% isoflurane. Rats were laid supine on a heating platform. Body temperature was monitored via a rectal thermometer (Indus Instruments, Houston, TX, USA) and maintained at 36.5°C to 37.5°C using a heating pad and lamp. The rat's chest was shaved and treated with a chemical hair remover to reduce ultrasound attenuation. To provide a coupling medium for the transducer, a warm ultrasound gel was spread over the chest wall. Transthoracic 2-dimensional, M-mode and Doppler imaging were performed with a high-resolution imaging system equipped with a 25-MHz transducer (VisualSonics, Toronto, ON, Canada). All echocardiographic parameters were calculated offline using tool section of the VisualSonics

Vevo770 System. All measurements were performed by an experienced sonographer in a blind manner.

2.4 Invasive hemodynamic measurement

The animals were initially anesthetized intraperitoneally with a mixture of ketamine (50 mg/kg) and medetomidin (100 μg/kg) for invasive hemodynamic measurements. A right-heart catheter was inserted through the right jugular vein for measurement of right ventricular mean pressure (RVMP), right ventricular systolic pressure (RVSP), mean pulmonary arterial pressure (mPAP), and the left carotid artery cannulation was performed for systemic arterial pressure (mSAP) and systolic body pressure (SBP) measurement. Total pulmonary resistance (TPR) was calculated by the ratio of mPAP/RVCO.

2.5 Histological analysis

Right ventricle and distal lungs were fixed in 4% paraformaldehyde, and then sectioned at 5-μm. Hematoxylin and eosin staining was used to determine cardiomyocyte hypertrophy and pulmonary artery media thickness (PAMT). The images of distal pulmonary arterioles per rat (diameter between 30 and 100 μm) were captured using a microscopic digital camera and analysis program (Becton Dickinson). The PAMT is defined as the distance between inner and outer elastic lamina. Vessel external diameter (ED) was determined. The relative PAMT (%) was calculated as 100×2PAMT/ED. The RV wall was separated from the left ventricular (LV) wall and ventricular septum (S). RV hypertrophy was expressed as the wet weight ratio of the RV wall and free LV wall with ventricular septum (RV/(LV+S)). RVWT was measured by

using a standard micrometer calliper (RVWT invasive).

2.6 Morphometric analysis of the lung vessels

Pulmonary vascular remodeling was measured by the degree of occlusion of capillary arteries on 7 μm-thick sections of frozen lung tissue. Slices were fixed with acetone for 10 min at room temperature and then saturated with human (10%) and donkey (10%) sera in PBS for 1 h at room temperature. Tissue sections were incubated for 24 h at 4°C with rabbit monoclonal anti-α-smooth muscle actin (α-SMA) antibody (1:100, Abcam, USA) and mouse monoclonal anti-NSD2 antibody (2 μg/ml, Abcam, USA). After washing, sections were incubated with Alexa Fluor 488 goat anti-mouse IgG (Invitrogen, Molecular Probes, Carlsbad, CA, USA; 1:2,000) and Alexa Fluor 594 goat anti-rabbit IgG (Invitrogen; 1:2,000) at room temperature for 1 h.

2.7 Western blot analysis

Tissues or cells were lysed in RIPA lysis buffer (50 mM Tris/HCl pH 7.4, 150 mM NaCl, 1% Nonidet P-40, 0.25% Na-eoxycholate, 1 mM EDTA and protease inhibitor cocktail) on ice for 30 min, and the lysates were collected by centrifugation at 12,000 rpm for 15 min at 4°C. The supernatants were collected and protein concentrations were determined using a BCA Protein Assay Kit (Beyotime, Jiangsu, China). Equal amounts of denatured proteins were subjected to SDS-PAGE and transferred onto PVDF membranes (Millipore, USA). The membranes were blocked with 5% non-fat dry milk in TBS-T (20 mM Tris, 137 mM NaCl, 0.05% Tween-20, pH 7.4) at room temperature for 3 h and then incubated with primary antibodies at 4°C

overnight. Subsequently, blots were washed and incubated with secondary antibodies at room temperature for 1 h. Finally, immuno-reactive bands were detected using an Odyssey Scanning system (Li-Cor, Lincoln, NE, USA).

2.8 Non-targeted LC-MS based metabolomics analysis

Samples stored at -80℃ were thawed at room temperature. 50 μl sample was mixed with 10 μl 2-chloro-l-phenylalanine (0.3 mg/ml) dissolved in methanol. Subsequently, 150 μl ice-cold mixture of methanol and acetonitrile (2/1, v/v) was added, and the mixtures were vortexed for 1 min, ultrasonicated at room temperature for 5 min, and stored at -20℃ for 10 min. The extract was centrifuged at 12,000 rpm at 4℃ for 10 min. 150 μl of supernatant in a glass vial was dried in a freeze concentration centrifugal dryer. 80 μl of 15 mg/ml methoxylamine hydrochloride in pyridine was subsequently added. The resultant mixture was vortexed vigorously for 2 min and incubated at 37℃ for 90 min. 80 μl of BSTFA (with 1% TMCS) and 20 μl n-hexane were added into the mixture, vortexed vigorously for 2 min and then derivatized at 70℃ for 60 min. The samples were placed at room temperature for 30 min before analysis on a GC-MS system (Agilent, model: 7890B) coupled with a mass selective detector (Agilent, model: 5977A). A DB-5MS fused-silica capillary column (30 m × 0.25 mm × 0.25 μm, Agilent J & W Scientific, Folsom, CA, USA) was utilized to separate the derivatives. The analysis was performed under the following conditions: Helium (> 99.999%) was used as the carrier gas at a constant flow rate of 1 mL/min through the column. The injector temperature was maintained at 260℃. Injection volume was 1 μl by splitless mode, and the solvent delay time was set to 5 min. The initial oven temperature was 50℃, ramped to

125℃ at a rate of 15℃/min, to 210℃ at a rate of 5℃/min, to 270℃ at a rate of 10℃/min, to 305℃ at a rate of 20℃/min, and finally held at 305℃ for 5 min. The temperature of MS quadrupole and electron impact ion source was set to 150℃ and 230℃, respectively. The collision energy was 70 eV. Mass spectrometric data were acquired in a full-scan mode (m/z 50-450). The QCs were injected at regular intervals (every 10 samples) throughout the analytical run to provide a set of data from which repeatability could be assessed.

2.9 Statistical analysis

All data were presented as mean±SD and analyzed by SPSS 11.0 statistical software. Differences among various treatment groups were compared by one-way ANOVA. Differences were considered significant at $P<0.05$.

3 Results

3.1 NSD2 silencing ameliorates MCT-induced PAH in rat model

To understand the role of NSD2 in MCT-induced PAH, SD rats were randomly divided into 4 groups (n=6): AAV-null treated SD rats administered with saline ($Null_{sham}$); AAV-null treated SD rats administered with MCT ($Null_{MCT}$); AAV-shNSD2 treated SD rats administered with saline ($shNSD2_{sham}$); and AAV-shNSD2 treated SD rats administered with MCT ($shNSD2_{MCT}$). As shown in Figure 1, MCT significantly increased RVMP, RVSP, mPAP, TPR, and PAMT (vs. saline treatment, $P<0.01$). RVCO in MCT treated groups was significantly reduced compared with saline treated groups ($P<0.01$), but there were no significant differences in SBP and mSAP between MCT and saline treated groups. Furthermore, NSD2 silencing led to

significant decreases in RVMP, RVSP, mPAP, TPR and PAMT in shNSD2$_{MCT}$ group compared with Null$_{MCT}$ group (P<0.01), and significant increases in RVCO in shNSD2$_{MCT}$ group compared with Null$_{MCT}$ group (P<0.01). Collectively, these data suggest that NSD2 silencing can ameliorate PAH in MCT-induced rat PAH model.

3.2 NSD2 silencing ameliorates right ventricular dysfunction in rat PAH model

Since PAH leads to dysfunction and failure of the right ventricle, we wonder whether NSD2 silencing ameliorates right ventricular dysfunction in rat PAH model. As shown in Figure 2, MCT significantly increased RVEDD, RVEDV, RVESD, RVESV, RVPWT and IVST (vs. saline treatment, P<0.01), and significantly decreased RVEF, RVFS and PAAT/CL (vs. saline treatment, P<0.01). NSD2 silencing effectively increased RVEDD, RVEDV, RVESD, RVESV, RVPWT and IVST, and reduced RVEF, RVFS and PAAT/CL in AAV-shRNA-NSD2 infected rats (vs. AAV-null, P<0.01). These data indicate that MCT-induced PAH rats develop right ventricular dysfunction, which could be ameliorated by NSD2 silencing.

3.3 NSD2 silencing partially reverses pathological remodeling of pulmonary artery and right ventricular hypertrophy

To confirm that NSD2 is involved in the remodeling of pulmonary arterial wall, we first compared the thickness of PA between Null$_{sham}$ and Null$_{MCT}$ group. We found significant increase of pulmonary arterial wall thickness in MCT treated rats compared with saline treated rats, but NSD2 silencing effectively inhibited the thickening of PA (Figure 3A, B). Additionally, we observed obvious hypertrophy of RV in MCT treated rats, but NSD2

silencing partially reversed RV hypertrophy. Quantitative analysis showed that RV/BW and RV/(LV+S) in MCT treated rats significantly increased compared with saline treated rats, but NSD2 silencing significantly decreased RV/BW and RV/(LV+S) (Figure 3C, D). Taken together, these data indicate that NSD2 silencing partially reverses pathological remodeling of pulmonary artery and right ventricular hypertrophy in PAH rat model induced by MCT.

3.4 NSD2 mediates the di-methylation of H3K36 in PAH model

Next, we examined whether NSD2-mediated methylation of H3K36 is involved in PAH. Immunofluorescence analysis of small size pulmonary artery showed that NSD2 was mainly expressed in SMCs in PA (Figure 4A). MCT significantly increased NSD2 expression, and NSD2 silencing significantly decreased protein expression of NSD2 in pulmonary artery sections (Figure 4B). Western blot analysis showed that NSD2 silencing markedly reduced the di-methylation level of H3K36 (H3K36me2), but there were no significant changes in H3K36me1, H3K36me3, H3K4me1, H3K4me2 and H3K4me3 levels in pulmonary artery sections (Figure 4B). Taken together, these data suggest that NSD2-mediated di-methylation of H3K36 is involved in PAH.

3.5 Metabolomic analysis of NSD2-mediated PAH

NSD2-mediated metabolic abnormality plays an essential role in oncogenesis. This phenomenon motivated us to detect NSD2-mediated metabolic alteration in lung tissue from rats with PAH and determine how the differentially expressed metabolites regulate PAH. Non-targeted LC-MS based metabolomics analysis of metabolites from rat lung tissue (Figure

5A) showed that trehalose was changed most significantly among $Null_{Sham}$, $Null_{MCT}$, $shNSD2_{Sham}$ and $shNSD2_{MCT}$ group (Figure 5B). Enrichment analysis of Kyoto encyclopedia of genes and genomes (KEGG) metabolic pathway indicated that NSD2-regulated trehalose mainly affected ABC transporters, mineral absorption, protein digestion and absorption, metabolic pathways and aminoacyl-tRNA biosynthesis (Figure 5C). Furthermore, network analysis showed that trehalose is closely related to ABC transporters and metabolic pathways (Figure 5D). Taken together, these data indicate that NSD2-mediated di-methylation of H3K36 regulates PAH via changing trehalose metabolism, which could affect ABC transporters and metabolic pathways.

3.6 NSD2 regulates autophagy in PAH

Enhanced autophagy has been indicated to contribute to PAH and PAH-induced ventricular hypertrophy[16,17]. Trehalose has been reported to induce autophagy in many diseases[18]. These findings promoted us to investigate whether NSD2-mediated change in trehalose metabolism may regulate autophagy in PAH. Western blot analysis showed that positive regulators of autophagy including LC3-II, beclin-1 and phos-AMPK were iupregulated while autophagy suppressor p62 was downregualted in $Null_{MCT}$ group compared with $Null_{Sham}$ group. Silencing of NSD2 markedly decreased the levels of LC3-II, beclin-1 and phos-AMPK, and increased p62 expression in $shNSD2_{MCT}$ group compared with $Null_{MCT}$ group (Figure 6). These data suggest that NSD2 might regulate autophagy in PAH via modulating trehalose metabolism.

4 Discussion

MCT-induced PAH rat model has significantly contributed to the understanding of PAH pathophysiology and the development of therapeutics[19]. In present study, we successfully established SD rat PAH model through intraperitoneal injection of MCT, which was evaluated via assessing haemodynamics and right ventricular function. Compared with the control groups, silencing of NSD2 by shRNA can improve right ventricular function, suppress right ventrivular hypertrophy, lower pulmonary arterial pressure and total pulmonary resistance and reverse pulmonary arterial remodeling in PAH model induced by MCT. Meanwhile, decrease in NSD2 expression achieved by NSD2 gene silencing was accompanied by reduced H3K36me2 level and autophagy. Furthermore, Non-targeted LC-MS based metabolomics analysis of lung tissue identified significant alteration in trehalose, which was significantly upregulated in MCT treated rats but was downregulated in NSD2 shRNA treated rats. Our study provides strong evidence that metabolic reprogramming mediated by NSD2 may play a vital role in the development of experimental rat PAH.

PAH is characterized by metabolic reprogramming, excessive proliferation, and apoptotic resistance of resident and recruited cells within the pulmonary arterial wall, sharing similar properties with cancer cells[21,22]. Metabolic alterations have been proposed to provide substrates and enzymes for increased biosynthesis to support cell survival and proliferation and thus have become emerging targets for novel diagnostic and therapeutic approaches that may have relevance to PAH. It has been demonstrated that abnormal proliferation of PASMC and EC plays a dominant role in the thickening of pulmonary arterial wall and the decrease in the pulmonary arterial lumen area[20-22]. In our study, MCT-induced rat PAH model showed thicker vessel wall and smaller lumen area than the control group, with the elevation of PAP

and PVR and dysfunction and hypertrophy of right ventricle. Numerous studies have shown that increased glycolysis is associated with the development of PAH. Overexpression of glycolytic enzymes, such as glucose transporter 1 (GLUT1), phosphofructokinase B3 (PFKB3), pyruvate dehydrogenase (PDH) kinase 1, and lactate dehydrogenase A (LDHA), may promote glycolysis and confer cells hyperproliferative and apoptosis resistant phenotype. For instance, alpha-enolase (ENO1), a glycolytic enzyme catalyzing the dehydration of 2-phospho-D-glycerate (2-PG) to phosphoenolpyruvate (PEP) in the glycolytic pathway, was elevated in lungs from patients with PAH[23]. Overexpression of ENO1 in PASMC induced de-differentiated and proliferative, apoptosis resistant and glycolytic phenotype, while the silencing or inhibition of ENO1 decreased PASMC proliferation, promoted differentiation and apoptosis, and restored the mitochondrial respiration[23]. Fatty acid metabolic defects also participate in the development of PAH and right ventricular dysfunction and hypertrophy. On one hand, reduced fatty acid oxidation can promote glucose oxidation, and thus mitigates the development of PAH[24]. On the other hand, reduced fatty acid oxidation will lead to lipid accumulation in the form of triglycerides, diacylglycerol, and ceramides in the cytoplasm of RV cardiomyocytes, causing lipotoxicity[25,26].

Accumulating evidence showed that elevated NSD2 plays a major role in the proliferation and survival of malignant cells. NSD2 upregulates the expression of genes critical for cell proliferation, anti-apoptosis and survival through catalyzing the di-methylation and/or tri-methylation of H3K36 (H3K36me2, H3K36me3) at the promoter of these genes[12,14,27]. Overexpression of NSD2 conferred breast cancer cells strong hormone-independent proliferative activities[12]. In addition, NSD2 promoted the proliferation of pancreatic β cells[27].

Consistently, knockdown of NSD2 resulted in a marked decrease of cell survival[12,28]. In this study, silencing of NSD2 showed inhibitory effects on the thickening of pulmonary arterial wall and right ventricle and protective role in pulmonary arterial pressure and right ventrivular function, suggesting that NSD2 might be involved in the proliferation and/or anti-apoptosis of cells within PA. Furthermore, the downregulation of NSD2 was accompanied by decreased level of H3K36me2, indicating that NSD2-meidated thickening of PA was achieved by increasing H3K36me2 level. Interestingly, NSD2 elevation strongly stimulated the expression of TIGAR, HK2, and G6PD via di-methylating H3K36 (H3K36me3) at the promoters, indicating its important role in metabolic reprogramming[12]. Elevated NSD2 strongly suppressed H_2O_2-induced ROS production and cell death/apoptosis. Consistently, knockdown of NSD2 or HK2 or G6PD or TIGAR strongly increased ROS level and cell death/apoptosis and decreased NADPH production[12]. HK2 plays a pivotal role in diversion of glucose into pathways such as the PPP for enhanced anabolic metabolism required for cell proliferation. G6PD is the rate-limiting enzyme of the PPP and plays a key role in NADPH production. TIGAR is a modulator of PPP, which was significantly decreased in NSD2-overexpressing cells. Enhanced PPP is usually associated with elevated synthesis of nucleosides or nucleotides. Indeed, metabolomics profiling demonstrated that NSD2-overexpressing cells had higher levels of multiple nucleosides.

Several studies have suggested that NAPDH, G6PD and PPP were involved in the development of PAH. Serving as a cofactor for nitric oxide synthase, NADPH plays a role in the initial phase of PH development for vasoconstriction of pulmonary arteries[29]. The activity of NADPH-producing isocitrate dehydrogenase-1 and -2 increased in pulmonary arteries and

lungs of idiopathic- and heritable-PAH patients [30]. G6PD is a major supplier of cellular NADPH. G6PD and G6PD derived NADPH mediate hypoxic pulmonary vasoconstriction. The expression and activity of G6PD is increased in endothelin-1-treated PASMCs from PAH patients, fibroblasts from idiopathic PAH patients and calves with severe hypoxic PH, ECs of monocrotaline treated mice and lungs of hypoxia-induced and monocrotaline-induced PAH rat models. Importantly, ectopic expression of G6PD increased rat PASMC proliferation[31] and contributed to HIF1a-induced EC growth[29]. It has been reported that G6PD and PPP activity increased before PH developed[31]. Expression of enzymes in the glycolytic pathway was upregulated in PASMCs from PAH patients[30]. Collectively, metabolic reprogramming is a key mechanism underlying oncogenesis and PAH, and NSD2 has been reported to regulate metabolic alterations in caner, indicating NSD2 may participate the development of PAH via reprogramming the metabolism.

Trehalose, a non-reducing disaccharide consisting of two glucose residues, is synthesized via the trehalose-6-phosphate synthase/trehalose phosphatase (TPS/TPP) pathway. Trehalose has an important role in protecting cells against oxidative stress, hypoxia and inflammatory responses: it could inhibit proinflammatory phenotype in macrophages[32]; downregulate inducible nitric oxide synthase (iNOS) and nitric oxide (NO) production in macrophages[33]; prevent angiogenesis by partially downregulating VEGF receptor 2 (VEGFR2) expression, which is an important mechanism underlying plexiform lesions[34]; inhibit the proliferation of myofibroblasts partially by inducing mesenchymal-epithelial transition[34]; inhibit H_2O_2-induced increase of intracellular ROS, endoplasmic reticulum (ER) stress and reduction in the activities of CAT and SOD[35]; decrease H_2O_2-induced autophagic death and oxidative

stress induced cell damage and apoptosis, and increase cell survival[35-37]. Our metabolic analysis showed that trehalose was increased in lung tissue from MCT-treated mice but decreased in NSD2 shRNA-treated mice. Although there is no evidence that trehalose can be synthesized by humans and other mammals, it was detected in rat lung tissue in this study. We speculate that trehaose will be absorbed from intestine and accumulate to significant levels in lung tissue with PAH. Certainly, detailed studies are needed to elucidate the role of trehalose in PAH and the mechanism underlying the correlation of trehalose with NSD2.

Increased autophagy has been reported in many diseases including PAH, and inhibition of autophagy can significantly prevent PAH progression by suppressing the proliferation and migration of PASMCs and inducing their apoptosis[17,38,39]. Interestingly, trehalose can induce autophagy in the liver, kidney, nervous system, vasculature and heart, inhibiting cell apoptosis[40-43]. In particular, trehalose can significantly improve cardiac remodeling, apoptosis and fibrosis by activating autophagy[40]. In addition, trehalose can enhance arterial endothelial cell autophagy, leading to reduced oxidative stress and inflammation and increased NO bioavailability[44]. Our data show that silencing of NSD2 can markedly decrease trehalose and reduce autophagy in lung tissue, suggesting that NSD2-mediated change in trehalose metabolism might participate in the development of PAH via regulating autophagy.

In summary, our study for the first time reveals that NSD2 participates in the development and progression of MCT-induced PAH via reprogramming metabolism of pulmonary vasculature. In our next plan, we will investigate the detailed mechanism by which NSD2 acts as an epigenetic regulator to modulate the expression of genes involved in metabolic reprogramming and further validate whether NSD2 is a promising target for PAH prevention

and treatment.

Author contribution

Xue-liang Zhou and Zhi-bo Liu performed molecular biology studies, Rong-rong Zhu, Huang Huang, Qi-rong Xu, Hua Xu, Liang Zeng, Yun-yun Li, Cha-hua Huang, and Qi-cai Wu performed animal studies, Ji-chun Liu designed the study. All authors read and approved the manuscript.

Acknowledgement

This work was supported by grants from the National Natural Science Foundation of China (No. 81860045, 81860054, 81560049, 81460065) and the Natural Science Foundation of Jiangxi Province (No. 20161BAB205256, 20181BAB205003).

Competing interests

The authors declare that they have no competing interests.

References

1 D'Alessandro A, El Kasmi KC, Plecita-Hlavata L, Jezek P, Li M, Zhang H, et al. Hallmarks of Pulmonary Hypertension: Mesenchymal and Inflammatory Cell Metabolic Reprogramming. Antioxidants & Redox Signaling 2018; 28:230-250

2 Harvey L, Chan S. Emerging Metabolic Therapies in Pulmonary Arterial Hypertension. Journal of Clinical Medicine 2017; 6:43

3 Archer SL, Fang YH, Ryan JJ, Piao L. Metabolism and bioenergetics in the right ventricle and pulmonary vasculature in pulmonary hypertension. Pulmonary Circulation 2013; 3:144-152

4 Xu W, Erzurum SC. Endothelial cell energy metabolism, proliferation, and apoptosis in pulmonary hypertension. Comprehensive Physiology 2011; 1:357-372

5 Ryan JJ, Archer SL. Emerging concepts in the molecular basis of pulmonary arterial hypertension: part I: metabolic plasticity and mitochondrial dynamics in the pulmonary circulation and right ventricle in pulmonary arterial hypertension. Circulation 2015; 131:1691-1702

6 Bennett RL, Swaroop A, Troche C, Licht JD. The Role of Nuclear Receptor-Binding SET Domain Family Histone Lysine Methyltransferases in Cancer. Cold Spring Harbor Perspectives in Medicine 2017; 7:a026708

7 Morishita M, Luccio ED. Cancers and the NSD family of histone lysine methyltransferases. Biochimica Et Biophysica Acta 2011; 1816:158-163

8 Kassambara A, Klein B, Moreaux J. MMSET is overexpressed in cancers: Link with tumor aggressiveness. Biochemical & Biophysical Research Communications 2009; 379:840-845

9 Hudlebusch HR, Santoni-Rugiu E, Simon R, Ralfkiær E, Rossing HH, Johansen JV, et al. The histone methyltransferase and putative oncoprotein MMSET is overexpressed in a large variety of human tumors. Clinical Cancer Research 2011; 17:2919-2933

10 Vougiouklakis T, Hamamoto R, Nakamura Y, Saloura V. The NSD family of protein methyltransferases in human cancer. Epigenomics 2015; 7:863-874

11 Hudlebusch HR, Skotte J, Santoni-Rugiu E, Zimling ZG, Lees MJ, Simon R, et al. MMSET is highly expressed and associated with aggressiveness in neuroblastoma. Cancer Research 2011; 71:4226-4235

12 Wang J, Duan Z, Nugent Z, Zou JX, Borowsky AD, Zhang Y, et al. Reprogramming metabolism by histone methyltransferase NSD2 drives endocrine resistance via coordinated activation of pentose phosphate pathway enzymes. Cancer Letters 2016; 378:69-79

13 Kuo AJ, Cheung P, Chen K, Zee BM, Kioi M, Lauring J, et al. NSD2 links dimethylation of histone H3 at lysine 36 to oncogenic programming. Molecular Cell 2011; 44:609-620

14 Yang P, Guo L, Duan ZJ, Tepper CG, Xue L, Chen X, et al. Histone Methyltransferase NSD2/MMSET Mediates Constitutive NF-κB Signaling for Cancer Cell Proliferation, Survival, and Tumor Growth via a Feed-Forward Loop. Molecular & Cellular Biology 2012; 32:3121-3131

15 Lu MH, Fan MF, Yu XD. NSD2 promotes osteosarcoma cell proliferation and metastasis by inhibiting E-cadherin expression. Eur Rev Med Pharmacol Sci 2017; 21:928-936

16 Rawat DK, Alzoubi A, Gupte R, Chettimada S, Watanabe M, Kahn AG, et al. Increased reactive oxygen species, metabolic maladaptation, and autophagy contribute to pulmonary arterial hypertension-induced ventricular hypertrophy and diastolic heart failure. Hypertension 2014; 64:1266-1274

17 Long L, Yang X, Southwood M, Lu J, Marciniak SJ, Dunmore BJ, et al. Chloroquine prevents progression of experimental pulmonary hypertension via inhibition of autophagy and lysosomal bone morphogenetic protein type II receptor degradation. Circulation

Research 2013; 112:1159-1170

18 Hosseinpour-Moghaddam K, Caraglia M, A. S. Autophagy induction by trehalose: Molecular mechanisms and therapeutic impacts. Journal of cellular physiology 2018; 233:6524-6543

19 Nogueira-Ferreira R, Vitorino R, Rita Ferreira R, Henriques-Coelho T. Exploring the monocrotaline animal model for the study of pulmonary arterial hypertension: A network approach. Pulmonary Pharmacology & Therapeutics 2015; 35:8-16

20 Zhuang W, Lian G, Huang B, Du A, Gong J, Xiao G, et al. CPT1 regulates the proliferation of pulmonary artery smooth muscle cells through the AMPK-p53-p21 pathway in pulmonary arterial hypertension. Molecular and Cellular Biochemistry 2018; Epub ahead of print

21 Su H, Xu X, Yan C, Shi Y, Hu Y, Dong L, et al. LncRNA H19 promotes the proliferation of pulmonary artery smooth muscle cells through AT1R via sponging let-7b in monocrotaline-induced pulmonary arterial hypertension. Respiratory Research 2018 19:254

22 Egnatchik RA, Brittain EL, Shah AT, Fares WH, Ford HJ, Monahan K, et al. Dysfunctional BMPR2 signaling drives an abnormal endothelial requirement for glutamine in pulmonary arterial hypertension. Pulmonary Circulation 2017; 7:186-199

23 Dai J, Zhou Q, Chen J, Rexius-Hall ML, Rehman J, Zhou G. Alpha-enolase regulates the malignant phenotype of pulmonary artery smooth muscle cells via the AMPK-Akt pathway. Nature Communications 2018; 9:3850

24 Sutendra G, Bonnet S, Rochefort G, Haromy A, Folmes KD, Lopaschuk GD, et al. Fatty

acid oxidation and malonyl-CoA decarboxylase in the vascular remodeling of pulmonary hypertension. Science Translational Medicine 2010; 2:44ra58

25 Talati M, Hemnes A. Fatty acid metabolism in pulmonary arterial hypertension: role in right ventricular dysfunction and hypertrophy. Pulmonary Circulation 2015; 5:269-278

26 Brittain EL, Talati M, Fessel JP, Zhu H, Penner N, Calcutt MW, et al. Fatty Acid Metabolic Defects and Right Ventricular Lipotoxicity in Human Pulmonary Arterial HypertensionClinical Perspective. Circulation 2016; 133:1936-1944

27 Shi S, Zhao L, Zheng L. NSD2 is downregulated in T2DM and promotes β cell proliferation and insulin secretion through the transcriptionally regulation of PDX1. Molecular Medicine Reports 2018 18:3513-3520

28 Guo MX, Zou Y, Lin LH, Ma XD, Huang YQ. Effects of Silencing NSD2 Gene by shRNA on Proliferation,Apoptosis and Akt /mTOR Signal Pathway in OCI-Ly3 Cells. Journal of Experimental Hematology 2018; 26:772-778

29 Leopold JA, Walker J, Scribner AW, Voetsch B, Zhang YY, Loscalzo AJ, et al. Glucose-6-phosphate Dehydrogenase Modulates Vascular Endothelial Growth Factor-mediated Angiogenesis The Journal of Biological Chemistry 2003; 278.:32100-32106

30 Yao C, Yu J, Taylor L, Polgar P, McComb ME, Costello CE. Protein expression by human pulmonary artery smooth muscle cells containing a BMPR2 mutation and the action of ET-1 as determined by proteomic mass spectrometry. International Journal of Mass Spectrometry 2015; 378:347-359

31 Chettimada S, Gupte R, Rawat D, Gebb SA, McMurtry IF, Gupte SA. Hypoxia-induced

glucose-6-phosphate dehydrogenase overexpression and -activation in pulmonary artery smooth muscle cells: implication in pulmonary hypertension. American Journal of Physiology Lung Cellular & Molecular Physiology 2015; 308:L287-L300

32 Minutoli L, Altavilla D, Bitto A, Polito F, Bellocco E, Laganà G, et al. The disaccharide trehalose inhibits proinflammatory phenotype activation in macrophages and prevents mortality in experimental septic shock. Shock 2007; 27:91-96

33 Espinosa-Cueto P, Escalera-Zamudio M, Magallanes-Puebla A, López-Marín LM, Segura-Salinas E, Mancilla R. Mycobacterial glycolipids di-O-acylated trehalose and tri-O-acylated trehalose downregulate inducible nitric oxide synthase and nitric oxide production in macrophages. BMC Immunology 2015; 16:38

34 Takeuchi K, Nakazawa M, Ebina Y. Effects of trehalose on VEGF-stimulated angiogenesis and myofibroblast proliferation: implications for glaucoma filtration surgery. Investigative Opthalmology & Visual Science 2011; 52:6987-6993

35 Gao Z, Wang H, Zhang B, Wu X, Zhang Y, Ge P, et al. Trehalose inhibits H2O2-induced autophagic death in dopaminergic SH-SY5Y cells via mitigation of ROS-dependent endoplasmic reticulum stress and AMPK activation. International Journal of Medical Sciences 2018; 15:1014-1024

36 Darabi S, Noori-Zadeh A, Abbaszadeh HA, Rajaei F. Trehalose Activates Autophagy and Prevents Hydrogen Peroxide-Induced Apoptosis in the Bone Marrow Stromal Cells. Iranian Journal of Pharmaceutical Research 2018; 17:1141-1149

37 Pan H, Ding Y, Yan N, Nie Y, Li M, Tong L. Trehalose prevents sciatic nerve damage to and apoptosis of Schwann cells of streptozotocin-induced diabetic C57BL/6J mice.

Biomedicine & Pharmacotherapy 2018 105:907-914

38 Yao Y, Li H, Da X, He Z, Tang B, Li Y, et al. SUMOylation of Vps34 by SUMO1 promotes phenotypic switching of vascular smooth muscle cells by activating autophagy in pulmonary arterial hypertension. Pulmonary pharmacology & therapeutics 2019; 55:38-49

39 Giraud-Billoud M, Fader CM, Agüero R, Ezquer F, Ezquer M. Diabetic nephropathy, autophagy and proximal tubule protein endocytic transport: A potentially harmful relationship. Biocell 2018;42: 35-40.

40 Sciarretta S YD, Nagarajan N, Bianchi F, Saito T, Valenti V, et al. Trehalose-Induced Activation of Autophagy Improves Cardiac Remodeling After Myocardial Infarction. Journal of the American College of Cardiology 2018; 71:1999-2010

41 Gong ZG WX, Wang JH, Fan RF, Wang L. Trehalose prevents cadmium-induced hepatotoxicity by blocking Nrf2 pathway, restoring autophagy and inhibiting apoptosis. Journal of Inorganic Biochemistry 2019; 192:62-71

42 Chou LF CY, Hsieh CY, Lin CY, Yang HY, Chen YC, et al. Effect of Trehalose Supplementation on Autophagy and Cystogenesis in a Mouse Model of Polycystic Kidney Disease. Nutrients 2018; 11:pii: E42

43 Pupyshev AB TM, Akopyan AA, Tenditnik MV, Dubrovina NI, Korolenko TA. Therapeutic activation of autophagy by combined treatment with rapamycin and trehalose in a mouse MPTP-induced model of Parkinson's disease. Pharmacology, biochemistry, and behavior 2019; 177:1-11

44 LaRocca TJ HG, Thorburn A, Sindler AL, Pierce GL, Seals DR. Translational evidence

that impaired autophagy contributes to arterial ageing. The Journal of physiology 2012; 590:3305-3316

Figure legends

Figure 1. NSD2 silencing ameliorates MCT-induced PAH in rat model. All data were presented as mean±SD (n=6).*P<0.05, **P<0.01.

Figure 2. NSD2 silencing effectively ameliorates right ventricular dysfunction in rat PAH model. All data were presented as mean±SD (n=6).*P<0.05, **P<0.01. *N.S*: not significant.

Figure 3. NSD2 silencing partially reverses pathological remodeling of pulmonary artery and right ventricular hypertrophy. A and B, RV hypertrophy was observed in MCT treated rats, which was reversed by silencing of NSD2 (vs. saline treatment, P<0.01). C and D, MCT-induced thickening of pulmonary arterial wall was partially reversed by NSD2 silencing (vs. AAV-null, P<0.01).

Figure 4. NSD2 regulates PAH via mediating the di-methylation of H3K36. A, Immunofluorescent staining of PA showed that NSD2 was mainly expressed in SMCs in PA. B, Western blot analysis of significant increase in NSD2 and H3K36me2 expression in pulmonary artery sections of MCT treated rats, while NSD2 silencing effectively decreased NSD2 and H3K36me2 expression (P<0.01).

Figure 5. Metabolomic analysis of NSD2-mediated PAH. A, Non-targeted LC-MS based metabolomics analysis of metabolites from rat lung tissue. B, Trehalose level was changed

most significantly among $Null_{Sham}$, $Null_{MCT}$, $shNSD2_{Sham}$ and $shNSD2_{MCT}$ group. C, Enrichment analysis of Kyoto encyclopedia of genes and genomes (KEGG) metabolic pathway. D, Network analysis of metabolites.

Figure 6. NSD2 regulates autophagy in PAH. Western blot analysis of the changes in the levels of autophagy markers in pulmonary artery sections of $Null_{Sham}$, $Null_{MCT}$, $shNSD2_{Sham}$ and $shNSD2_{MCT}$ group. GAPDH was loading control. All data were presented as mean±SD (n=6). *P<0.05, **P<0.01.

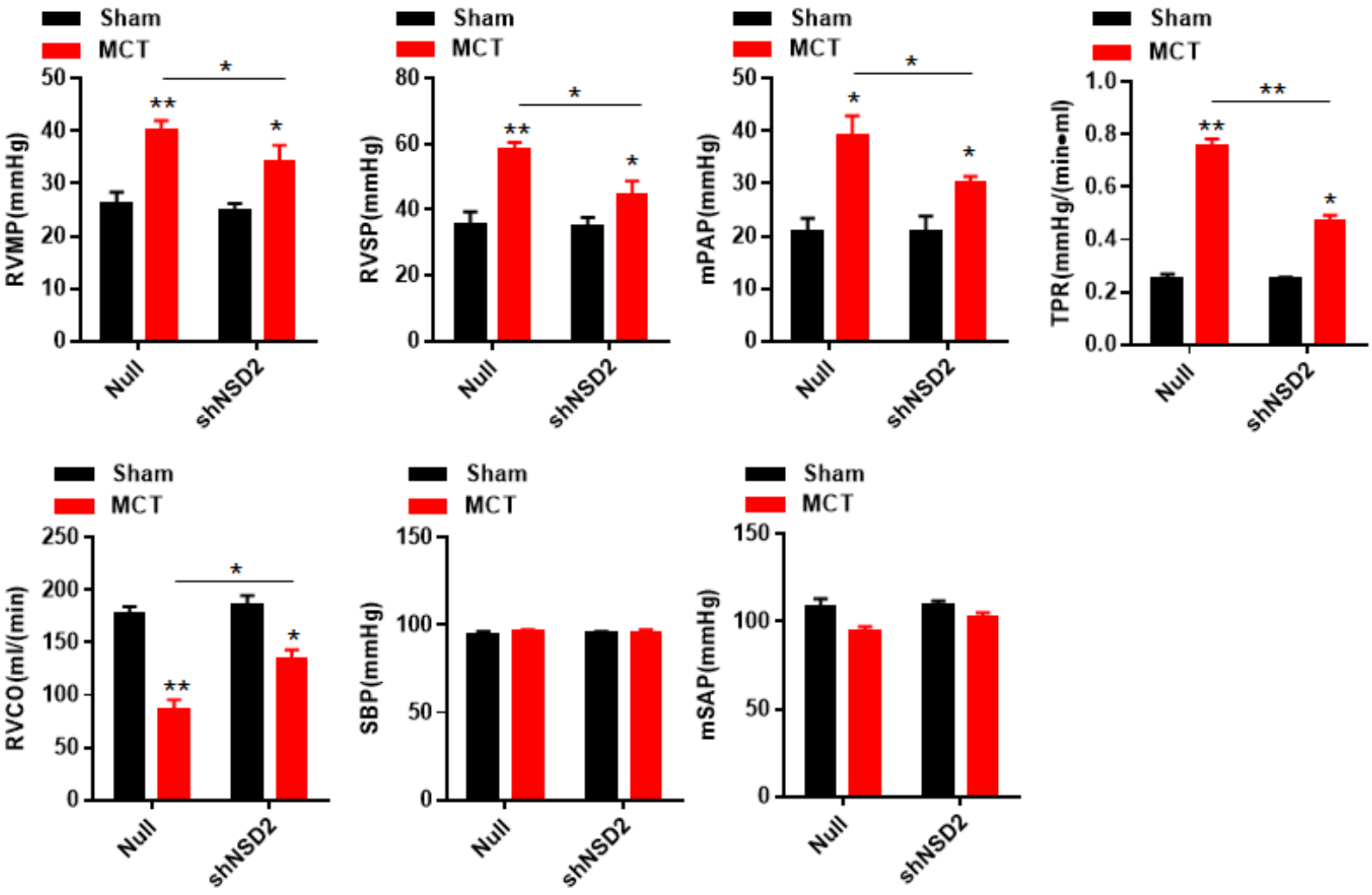
Sham
MCT
RVMP(mmHg)
RVSP(mmHg)
mPAP(mmHg)
TPR(mmHg/(min•ml))
RVCO(ml/(min)
SBP(mmHg)
mSAP(mmHg)
Null
shNSD2
*
**

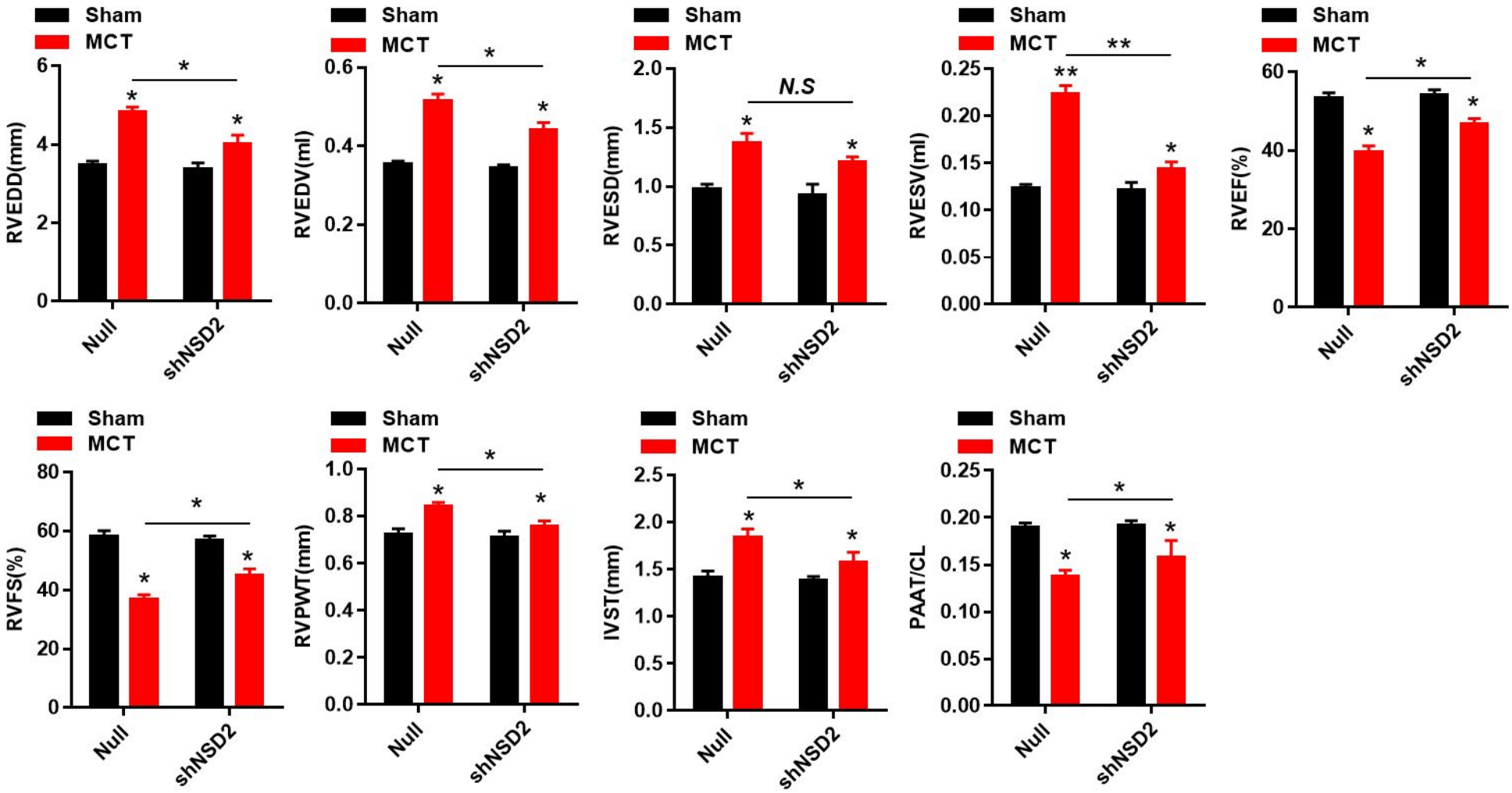
Sham
MCT
RVEDD(mm)
RVEDV(ml)
RVESD(mm)
RVESV(ml)
RVEF(%)
RVFS(%)
RVPWT(mm)
IVST(mm)
PAAT/CL
N.S
Null
shNSD2

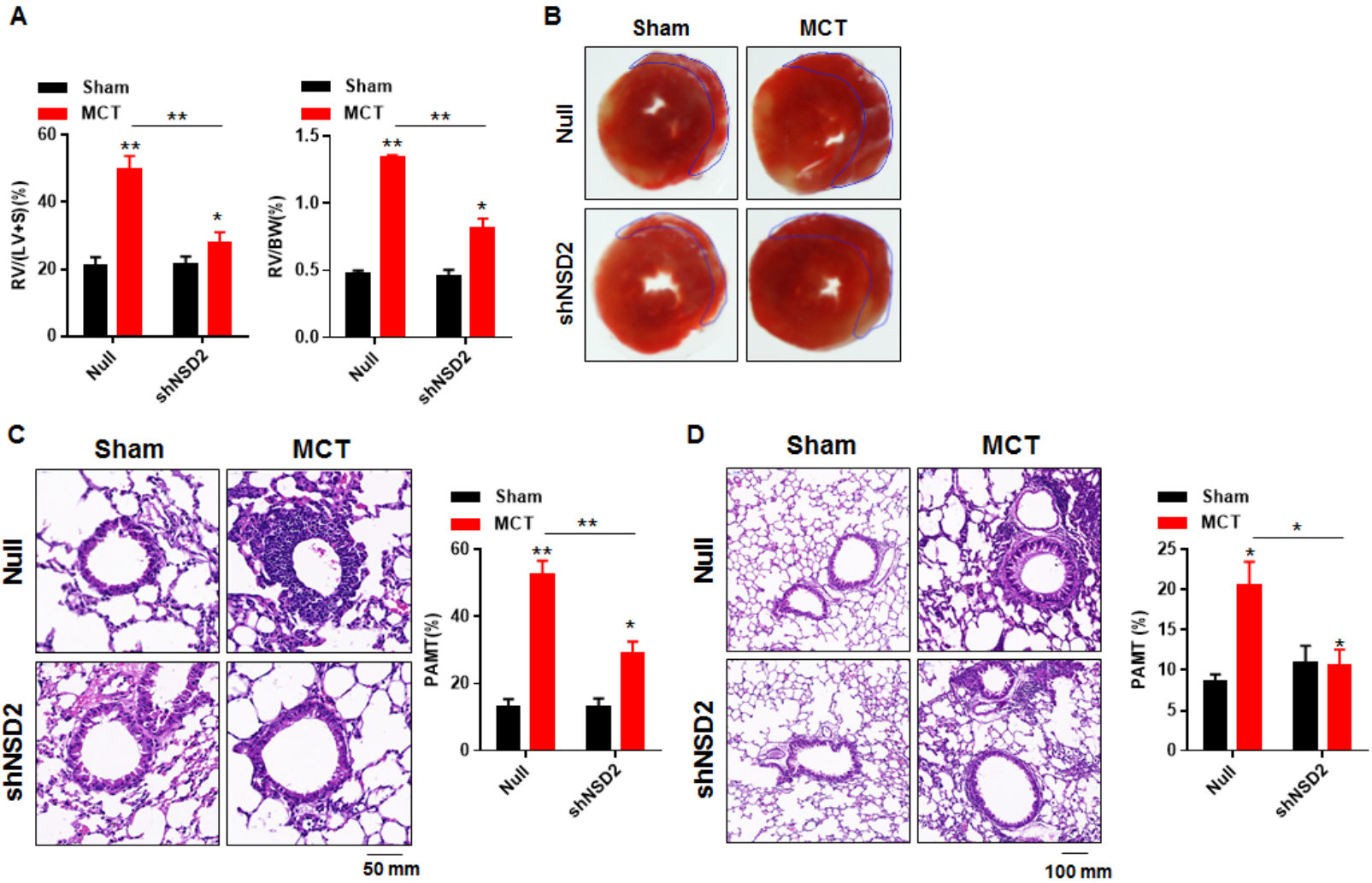
A
Sham
MCT
**
RV/(LV+S)(%)
60
40
20
0
**
*
Null
shNSD2
Sham
MCT
**
RV/BW(%)
1.5
1.0
0.5
0.0
**
*
Null
shNSD2
B
Sham
MCT
Null
shNSD2
C
Sham
MCT
Null
shNSD2
50 mm
Sham
MCT
**
PAMT(%)
60
40
20
0
**
*
Null
shNSD2
D
Sham
MCT
Null
shNSD2
100 mm
Sham
MCT
*
PAMT (%)
25
20
15
10
5
0
*
*
Null
shNSD2

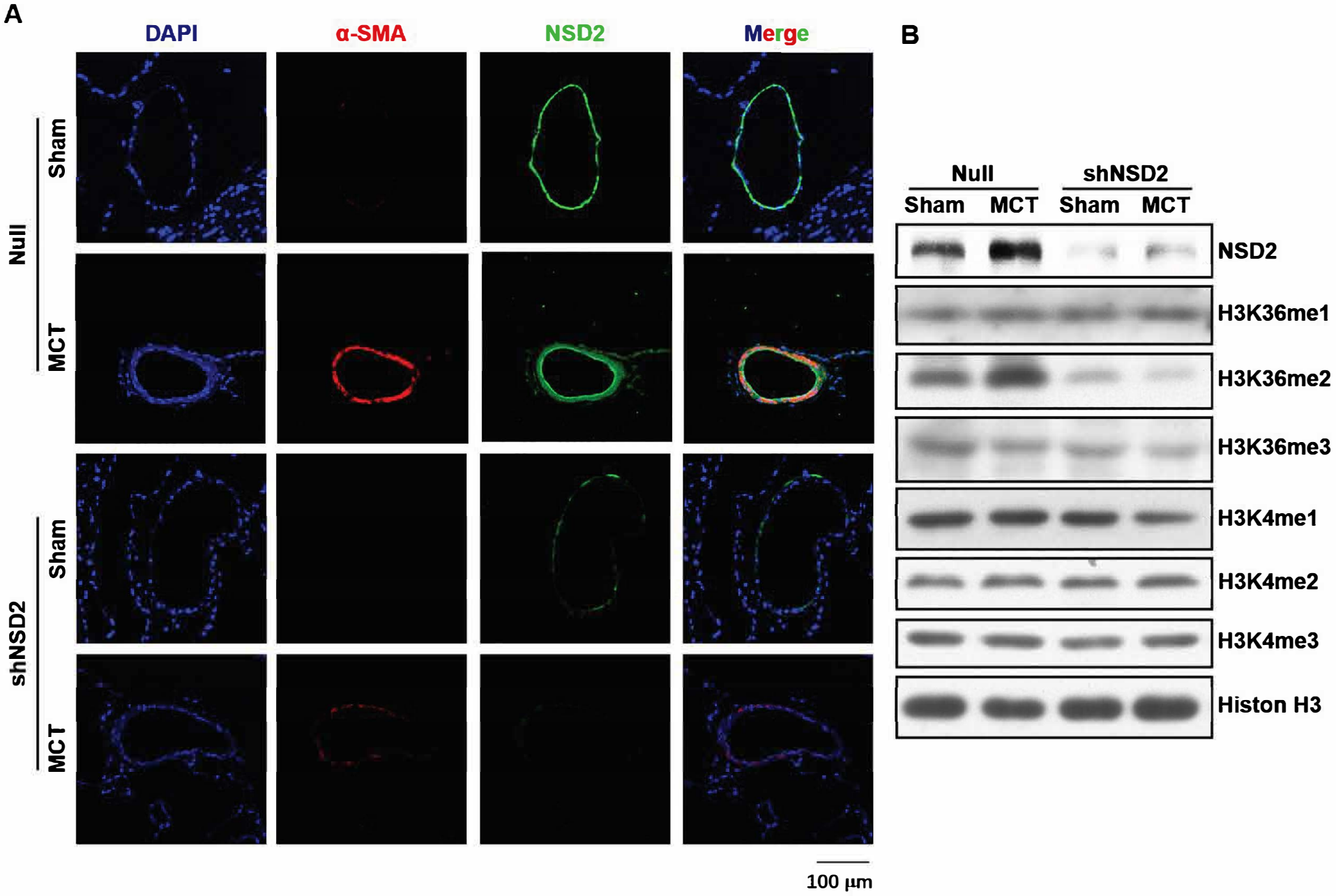
A
DAPI
α-SMA
NSD2
Merge
Null
Sham
MCT
shNSD2
Sham
MCT
100 μm
B
Null
shNSD2
Sham
MCT
Sham
MCT
NSD2
H3K36me1
H3K36me2
H3K36me3
H3K4me1
H3K4me2
H3K4me3
Histon H3

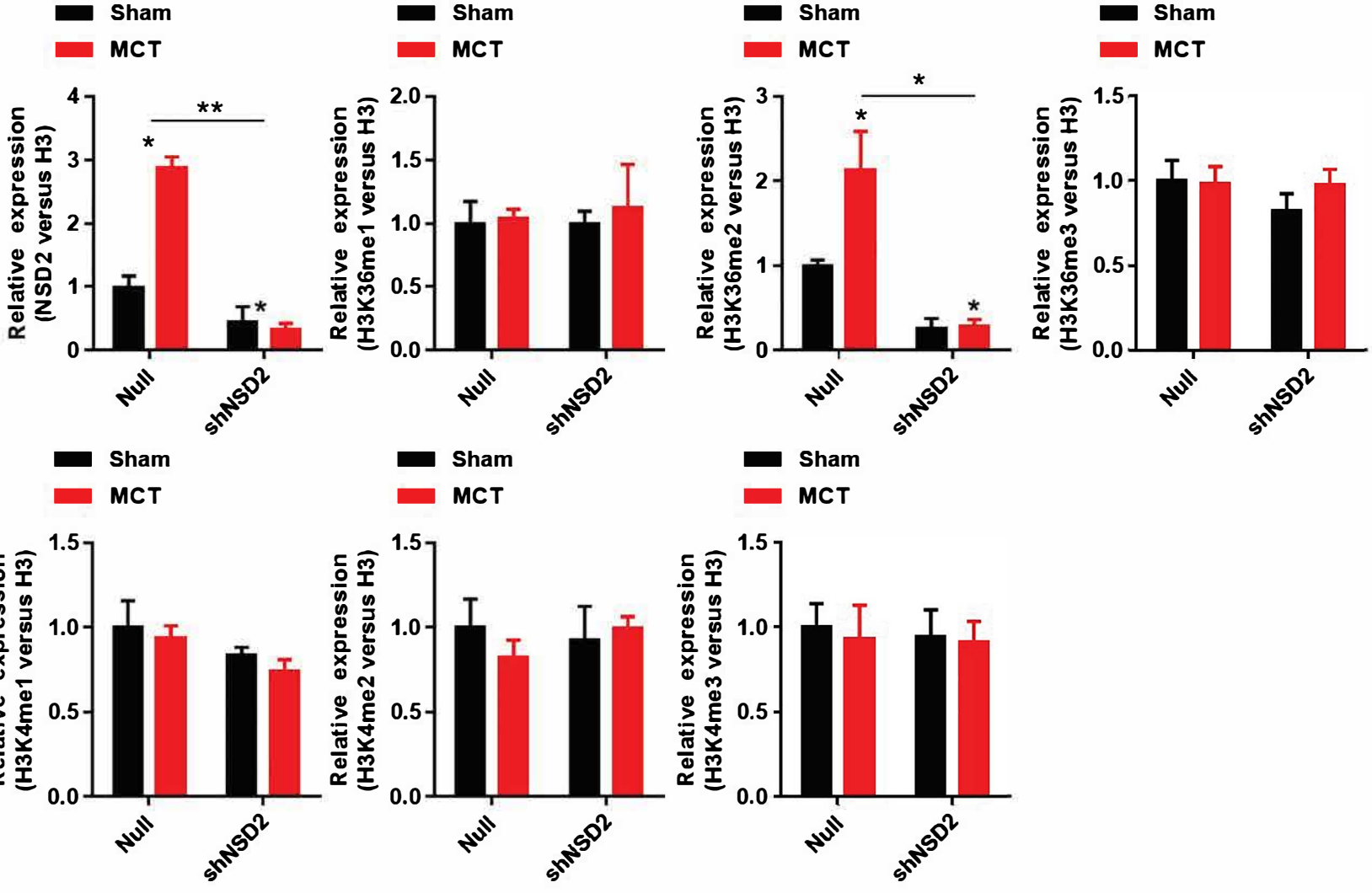
Sham
MCT
Relative expression (NSD2 versus H3)
Relative expression (H3K36me1 versus H3)
Relative expression (H3K36me2 versus H3)
Relative expression (H3K36me3 versus H3)
Relative expression (H3K4me1 versus H3)
Relative expression (H3K4me2 versus H3)
Relative expression (H3K4me3 versus H3)
Null
shNSD2
*
**

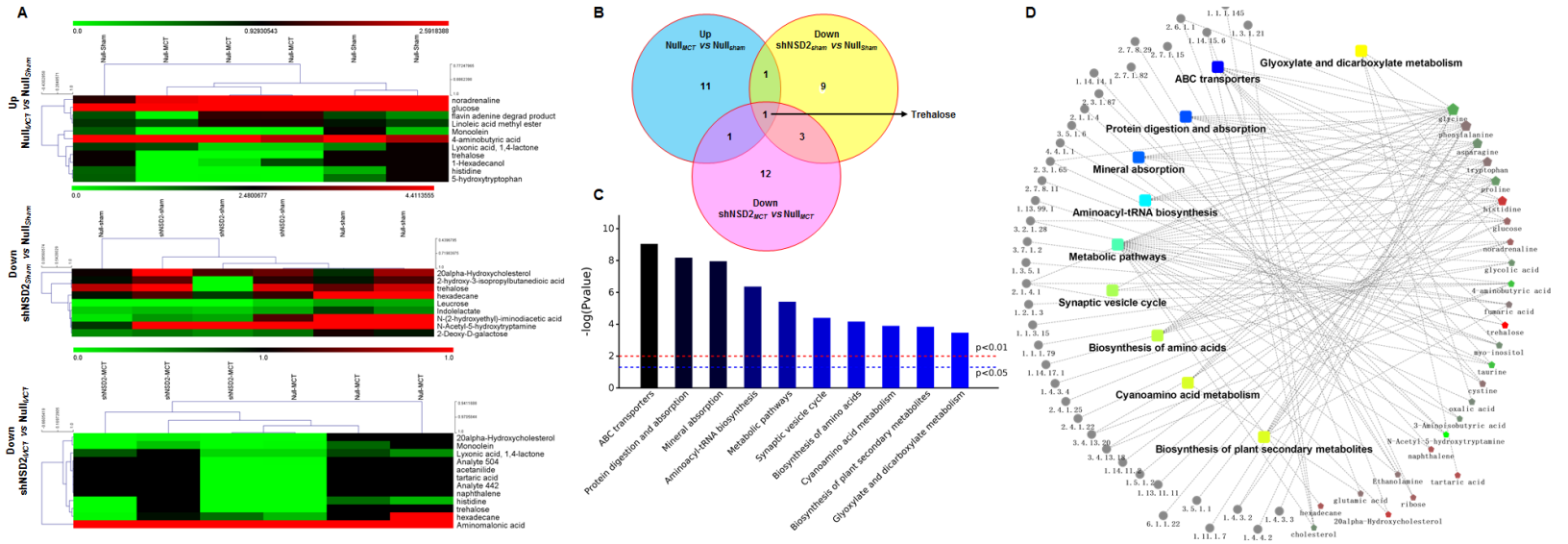
A
Up
Null_MCT vs Null_Sham
Null-Sham
Null-MCT
noradrenaline
glucose
flavin adenine degrad product
Linoleic acid methyl ester
Monoolein
4-aminobutyric acid
Lyxonic acid, 1,4-lactone
trehalose
1-Hexadecanol
histidine
5-hydroxytryptophan
Down
shNSD2_Sham vs Null_Sham
sNSD2-sham
Null-sham
20alpha-Hydroxycholesterol
2-hydroxy-3-isopropylbutanedioic acid
trehalose
hexadecane
Leucrose
Indolelactate
N-(2-hydroxyethyl)-iminodiacetic acid
N-Acetyl-5-hydroxytryptamine
2-Deoxy-D-galactose
Down
shNSD2_MCT vs Null_MCT
sNSD2-MCT
Null-MCT
20alpha-Hydroxycholesterol
Monoolein
Lyxonic acid, 1,4-lactone
Analyte 504
acetanilide
tartaric acid
Analyte 442
naphthalene
histidine
trehalose
hexadecane
Aminomalonic acid
B
Up
Null_MCT vs Null_sham
Down
shNSD2_sham vs Null_Sham
Down
shNSD2_MCT vs Null_MCT
11
1
9
1
1
3
12
Trehalose
C
-log(Pvalue)
p<0.01
p<0.05
ABC transporters
Protein digestion and absorption
Mineral absorption
Aminoacyl-tRNA biosynthesis
Metabolic pathways
Synaptic vesicle cycle
Biosynthesis of amino acids
Cyanoamino acid metabolism
Biosynthesis of plant secondary metabolites
Glyoxylate and dicarboxylate metabolism
D
Glyoxylate and dicarboxylate metabolism
ABC transporters
Protein digestion and absorption
Mineral absorption
Aminoacyl-tRNA biosynthesis
Metabolic pathways
Synaptic vesicle cycle
Biosynthesis of amino acids
Cyanoamino acid metabolism
Biosynthesis of plant secondary metabolites
glycine
phenylalanine
asparagine
tryptophan
proline
histidine
glucose
noradrenaline
glycolic acid
4-aminobutyric acid
fumaric acid
trehalose
myo-inositol
taurine
cystine
oxalic acid
3-Aminoisobutyric acid
N-Acetyl-5-hydroxytryptamine
naphthalene
Ethanolamine
tartaric acid
glutamic acid
ribose
hexadecane
20alpha-Hydroxycholesterol
cholesterol

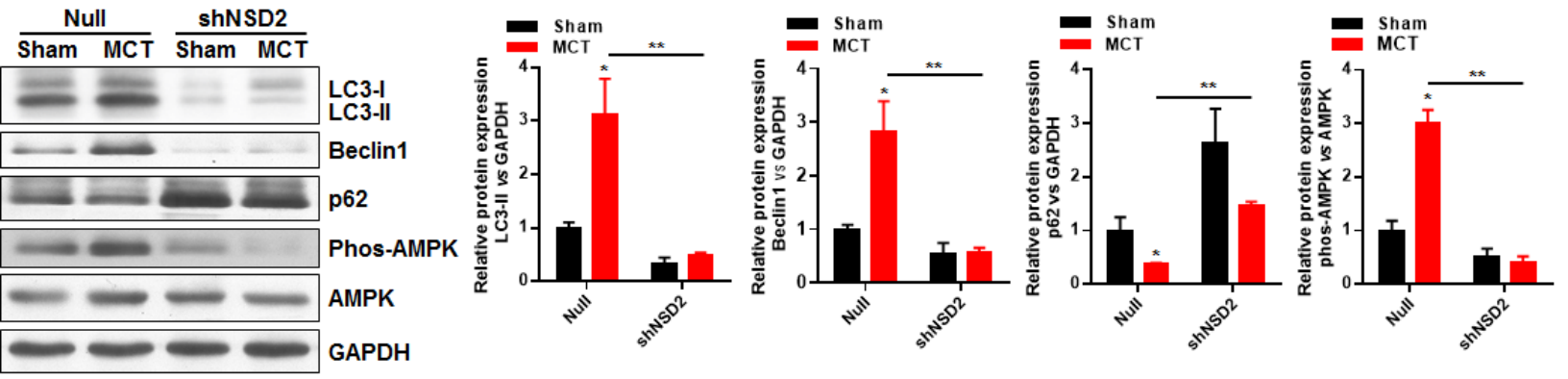
Null
shNSD2
Sham
MCT
Sham
MCT
LC3-I
LC3-II
Beclin1
p62
Phos-AMPK
AMPK
GAPDH
Sham
MCT
Relative protein expression
LC3-II vs GAPDH
Null
shNSD2
Relative protein expression
Beclin1 vs GAPDH
Relative protein expression
p62 vs GAPDH
Relative protein expression
phos-AMPK vs AMPK
*
**
0
1
2
3
4